Partial event coincidence analysis for distinguishing direct and indirect coupling in functional network construction

Jiamin Lu, (iD) Reik V. Donner, Dazhi Yin, et al.

View Online   **Export Citation**   **CrossMark**

ARTICLES YOU MAY BE INTERESTED IN
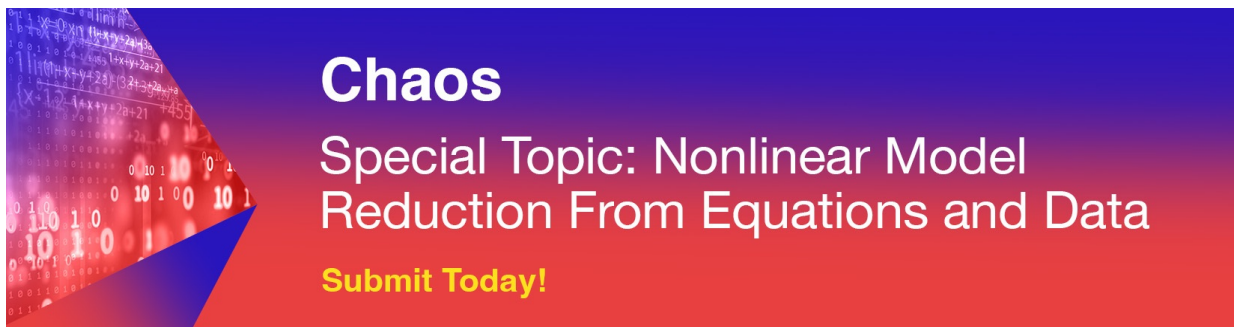
Chaos
Special Topic: Nonlinear Model Reduction From Equations and Data
Submit Today!

Partial event coincidence analysis for distinguishing direct and indirect coupling in functional network construction

View Online   Export Citation   CrossMark

Jiamin Lu,[1] Reik V. Donner,[2,3] [ID] Dazhi Yin,[4] Shuguang Guan,[1,a)] [ID] and Yong Zou[1,a)] [ID]

AFFILIATIONS

[1] School of Physics and Electronic Science, East China Normal University, Shanghai 200062, China
[2] Department of Water, Environment, Construction and Safety, Magdeburg–Stendal University of Applied Sciences, Breitscheidstraße 2, 39114 Magdeburg, Germany
[3] Potsdam Institute for Climate Impact Research (PIK) – Member of the Leibniz Association, Telegrafenberg A31, 14473 Potsdam, Germany
[4] Key Laboratory of Brain Functional Genomics (Ministry of Education and Shanghai), School of Psychology and Cognitive Science, East China Normal University, Shanghai 200062, China

[a)] Authors to whom correspondence should be addressed: sgguan@phy.ecnu.edu.cn and yzou@phy.ecnu.edu.cn

ABSTRACT

Correctly identifying interaction patterns from multivariate time series presents an important step in functional network construction. In this context, the widespread use of bivariate statistical association measures often results in a false identification of links because strong similarity between two time series can also emerge without the presence of a direct interaction due to intermediate mediators or common drivers. In order to properly distinguish such direct and indirect links for the special case of event-like data, we present here a new generalization of event coincidence analysis to a partial version thereof, which is aimed at excluding possible transitive effects of indirect couplings. Using coupled chaotic systems and stochastic processes on two generic coupling topologies (star and chain configuration), we demonstrate that the proposed methodology allows for the correct identification of indirect interactions. Subsequently, we apply our partial event coincidence analysis to multi-channel EEG recordings to investigate possible differences in coordinated alpha band activity among macroscopic brain regions in resting states with eyes open (EO) and closed (EC) conditions. Specifically, we find that direct connections typically correspond to close spatial neighbors while indirect ones often reflect longer-distance connections mediated via other brain regions. In the EC state, connections in the frontal parts of the brain are enhanced as compared to the EO state, while the opposite applies to the posterior regions. In general, our approach leads to a significant reduction in the number of indirect connections and thereby contributes to a better understanding of the alpha band desynchronization phenomenon in the EO state.

Published under an exclusive license by AIP Publishing. https://doi.org/10.1063/5.0087607

Functional network representations have recently gained considerable interest in the study of real-world spatially extended dynamical systems like the Earth's climate or the human brain. In a vast fraction of cases, the existence of network links has been established by resorting to the presence of strong bivariate statistical associations as suggested by symmetric association measures like classical linear (Pearson) correlations. This methodology, however, disregards two relevant aspects: the directionality of dynamical interactions between pairs of actors and the complexity of mutual (synergistic or antagonistic) inter-dependencies that can lead to the spurious identification of connections in case of, for example, common drivers or directed chain-like coupling configurations. In order to address both aspects, various approaches based on nonlinear time series analysis have been developed in the last few years, most of which assume the presence of a continuous temporal variability pattern. However, in the context of event-like data like spikes in neural activity or climate extremes, there still exists a considerable gap in suitable methodologies for unravelling the complex web of directed interactions from multivariate time series. The present work

introduces partial event coincidence analysis as a new approach and studies its applicability to different types of model systems as well as real-world EEG data.

I. INTRODUCTION

Over the last few decades, complex networks[1–3] have emerged as a powerful concept for describing structural or dynamical linkages among mutually interacting units across a broad range of scientific disciplines, including diverse fields like sociology, transportation systems, computer sciences, or ecology. Particularly important applications of complex network theory can be found in the context of functional network analysis, for example, of functional brain networks.[4] Other than the microscopic anatomic connectivity patterns of the brain (at the level of individual neurons or groups thereof), such functional networks are exclusively based on statistical linkages among multivariate neurophysiological recordings like multi-channel electroencephalography (EEG), magnetoencephalography (MEG), or functional Magnetic Resonance Imaging (fMRI), where the individual time series represent the macroscopic activity patterns in distant brain regions as reflected by electrical, magnetic, or blood oxygen level dependent signals, respectively. In such cases, the respective strengths of bivariate statistical associations between all pairs of series are taken as proxies for the likelihood of the existence of functional linkages between the two brain regions represented by the two series, which in their entirety describe a network structure. Similar functional network approaches are also utilized for identifying long distance interaction patterns in the global climate system.[5–9] Here, the motivation of this functional climate network analysis is to better understand and describe climate phenomena of interest. Besides various primarily diagnostic studies, recent applications of functional climate networks also include complex network based algorithms to predict the emergence and properties of specific climate phenomena like El Niño events, the Indian summer monsoon, or drought episodes in South America,[10] opening a new door for further development of statistical forecasting methods.

The critical step in functional network analysis of an arbitrary given multivariate data set is to infer the connection topology among the represented entities, which is essential for understanding the characteristic properties of the underlying complex system as a whole. For this purpose, previous works have proposed a vast suite of concepts to quantify statistical interrelationships between different time series (associated with, e.g., different brain regions), ranging from linear to nonlinear methods and including symmetric measures like linear Pearson correlation,[5,11] mutual information,[6] or event synchronization strength[12] as well as directed characteristics like Granger causality or transfer entropy.[13] However, exploiting conventional bivariate measures for coupling inference bears a high risk of associating strong statistical associations with links that are not present in reality. Indeed, beyond direct connections complex coupling configurations can easily lead to strong statistical associations even when two units are not directly interconnected. Take, for example, the two paradigmatic topologies of a star and a chain shown in Fig. 1, both of which exhibit both direct and indirect coupling between the network's nodes. For the star configuration
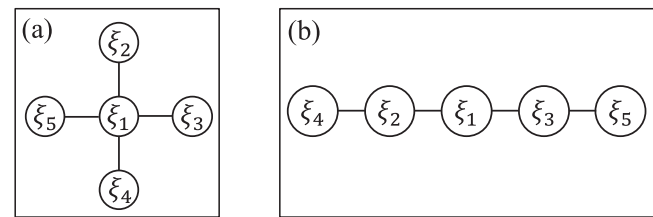

FIG. 1. Two exemplary coupling configurations with both direct and indirect interactions: (a) star and (b) chain.

[Fig. 1(a)], all connections among pairs of leaf nodes (ξ_2, ξ_3, ξ_4, and ξ_5) are indirect, while all connections between the hub ξ_1 and any of the leaves are direct. Similar observations apply to non-adjacent vs adjacent pairs of nodes in the chain [Fig. 1(b)].

In both exemplary configurations, indirect coupling between two nodes can result in strong dynamical similarity and, consequently, the false identification of a direct link based on traditional bivariate similarity measures. Therefore, it is important to empirically distinguish indirect from direct couplings. The task becomes particularly challenging and relevant in situations where the network structure to be inferred is spatially embedded, in which case short geodesic distances between units are commonly accompanied by a higher degree of dynamical similarity.

In order to eliminate the effect of possible pseudo-connections, several approaches have been developed in the last few years.[14,15] The probably most sophisticated one is the causal effect network analysis based on the Peter and Clark momentary conditional independence algorithm, which draws upon the concept of graphical models of time series to iteratively exclude indirect couplings from the set of possible "causal" (time-lagged) connections by exploiting partial correlations or conditional mutual information with systematically varying sets of conditioning variables.[16–18] Other recent works have taken simplified conditioning approaches while replacing the aforementioned more traditional conditional association measures by conditional ordinal pattern co-occurrence frequencies.[19,20] In the context of the present work, we particularly emphasize the exploitation of partial spectral coherence and partial phase synchronization/coherence,[7,21–23] both aiming at revealing direct connections by correcting bivariate association measures for the influence of other processes. The latter approach has been shown to distinguish direct from indirect coupling provided that the coupled systems show proper oscillatory behavior such that phase variables can be defined in a meaningful manner. However, there may be practically relevant cases where coupling is to be identified based exclusively on the timing of distinct events (e.g., for spike-like neuronal activity, climate extremes, or discrete spreading processes leading to cascading events).[8,24]

This paper introduces an advanced methodology for inferring network topology exclusively from the timing of events at different units (i.e., in different time series) by exploiting an analog of partial coherence analysis for event time series. In general, it is not straightforward to apply the nonlinear methods of phase synchronization analysis to the particular case of event time series, since the necessary definition of a phase variable is not unique and involves

a specific choice of temporal interpolation.[25] As potential alternatives specifically tailored to event time series, concepts like event synchronization (ES)[12] and event coincidence analysis (ECA)[26] have been proposed to uncover the nonlinear inter-dependency between two interacting complex systems exclusively based on the timing of distinct events. Both ES and ECA have found various applications to diverse fields of research, including EEG recordings,[12] human interaction patterns,[27] and climate extreme events.[9,28] Recent comparisons between ES and ECA have revealed typical situations in which the functional network structures derived using both methods can differ significantly,[24,29,30] particularly depending on the degree of temporal clustering of events. Here, we draw upon the approach underlying partial phase synchronization analysis to generalize the traditional bivariate ECA to a partial version thereof, aiming to distinguish direct from indirect interactions among event time series.

In order to demonstrate the potentials of the proposed methodology, we first discuss its utility by studying two types of numerically generated event time series on different generic coupling configurations without and with consideration of a two-dimensional spatial embedding. Subsequently, we disclose the distinct roles of direct and indirect connections in functional brain networks reconstructed from healthy human resting state alpha band EEG recordings under eyes open (EO) and eyes closed (EC) conditions.[31] In both cases, direct connections are found to exist primarily between neighbouring brain areas while indirect ones are mainly identified between brain regions that are separated by larger spatial distances. Taking only the direct connections into account, we find enhanced connection strengths in the frontal areas under EC as compared to EO conditions, while the connectivity under EO conditions becomes stronger in the posterior regions relative to the values in the EC state. The corresponding redistribution process could be relevant for better understanding the previously reported alpha band desynchronization in EO state.[32]

The remainder of this paper is organized as follows: in Sec. II, we present a generalization of ECA from classical bivariate to partial analysis. In Sec. III, we compare the results of this partial event coincidence analysis (PECA) with those of partial phase synchronization analysis for three noisy Rössler systems exhibiting both direct and indirect links. Subsequently, numerical results of PECA for coupled chaotic and stochastic models without and with two-dimensional spatial embedding are presented for the two coupling configurations shown in Fig. 1, which allow us to correctly distinguish direct from indirect coupling. Finally, we evaluate the coupling identification in functional brain network representations obtained from resting state multi-channel alpha-band EEG measurements in Sec. IV. Additional consistent results obtained from other independent EEG data sets are further detailed in the supplementary material.

II. METHODS

Event coincidence analysis (ECA) is a statistical method to measure similarities between event time series incorporating a predefined coincidence interval.[26] An event series is defined as an ordered set of N event timings $\{t_1, \ldots, t_N\}$. For example, in the case of a single-channel EEG time series $x_i(t)$ measured by one electrode i, an event takes place when $x_i(t)$ becomes larger than a threshold,

e.g., $x_e = \bar{x} + 1.8\sigma_x$, where $\bar{x}$ and σ_x are the mean and standard deviation of the signal x, respectively. The choice of the threshold depends on the particular time series under study, e.g., it may even not be necessary at all in some practical cases where spiking times are directly recorded. For instance, abrupt spiking events are genuine properties of tasked based or epileptic brain EEG recordings. In case of successive time steps for which x exceeds the predefined threshold value, the first one is commonly associated with the event of interest. Accordingly, a pair of event time series associated with two variables or units i and j is defined as two ordered event sets of size N_i and N_j, respectively, and we denote as t_l^i the time of event l in time series i and as t_m^j the time of event m in time series j with $l = 1, 2, \ldots, N_i$ and $m = 1, 2, \ldots, N_j$.[29]

A. Bivariate event coincidence analysis

ECA is based on the computation of event coincidence rates between two given event time series, i.e., the rates with which events in one variable occur in temporal proximity with those in the other. In order to define this proximity and, hence, mutual synchrony between events, a coincidence window needs to be specified first, which is evaluated relative to each individual event in one of the series that acts as the reference for the definition of event coincidence rates. This implies that these rates are not necessarily symmetric quantities and commonly change their values when the role of the reference series is exchanged among the two time series under study. Under general conditions, the coincidence window can be described by its start and end time relative to an event in the reference series, i.e., $[T^{(-)}, T^{(+)}]$, while the most common choices consider coincidence windows that are either completely in the past of an event (i.e., $[-\Delta T, 0]$), completely in its future (i.e., $[0, \Delta T]$), or combine both in a symmetric fashion with respect to the timing of an event (i.e., $[-\Delta T, \Delta T]$). In addition, we may further consider a systematic time shift of one series relative to the other by a time lag τ in the same fashion as, e.g., used in standard cross-correlation functions.

Disregarding the symmetric definition of a coincidence window, we consider here two versions of event coincidence rates. Specifically, we are interested in the fraction of cases where events in j precede (follow) events in i, which could be indicative of a possible causal influence from j to i (i to j). (The other direction from i to j is obtained by simply exchanging i and j in all formulas below.) In this case, two events at t_l^i and t_m^j are considered to coincide if $0 \leq t_l^i - t_m^j \leq \Delta T$. In addition, a proper time lag $\tau \geq 0$ between i and j can be incorporated by the condition $0 \leq (t_l^i - \tau) - t_m^j \leq \Delta T$.

To quantify the strength of statistical interrelationships between two event time series, we compute their precursor event coincidence rate that quantifies the fraction of events in i that are preceded by events in j as[26,29]

$$r_p(i|j; \Delta T, \tau) = \frac{1}{N_i} \sum_{l=1}^{N_i} \Theta \left[\sum_{m=1}^{N_j} 1_{[0, \Delta T]}((t_l^i - \tau) - t_m^j) \right], \quad (1)$$

and the trigger event coincidence rate measuring the fraction of events in j that are followed by events in i as

$$r_t(i|j; \Delta T, \tau) = \frac{1}{N_j} \sum_{m=1}^{N_j} \Theta \left[\sum_{l=1}^{N_i} 1_{[0,\Delta T]}((t_l^i - \tau) - t_m^j) \right], \quad (2)$$

where $1_{[0,\Delta T]}(\bullet)$ is the indicator function of the coincidence window defined by the maximum temporal event distance ΔT. As suggested by Odenweller and Donner,[29] in what follows we will use a single statistical association measure Q_{ij} that we will refer to as the *event coincidence strength* to characterize the degree of event synchrony, which is given by the mean of the two (directed) trigger event coincidence rates $r_t(i|j; \Delta T, \tau)$ and $r_t(j|i; \Delta T, \tau)$. We note that an analogous construction could be performed based on the two (directed) precursor event coincidence rates $r_p(i|j; \Delta T, \tau)$ and $r_p(j|i; \Delta T, \tau)$, which can be expected to result in somewhat different values, especially if the considered coupling is not bi-directional. Exploiting the corresponding asymmetries for extending the approach proposed in the following to the problem of differentiating between uni- and bidirectional coupling may provide an interesting research avenue for future research, but is beyond the scope of the present work. Therefore, we focus in the following on the event coincidence strength defined based on the symmetrization of pairs of trigger event coincidence rates.

Furthermore, it is notable that the definition of the underlying event coincidence rates features two parameters. In the present work, we exclusively utilize ΔT, which allows for events that do not exactly coincide in time between a pair of considered time series due to non-identical event definitions, sampling coarseness, or uncertainty due to stochastic components in the time series. By contrast, the second parameter τ, which allows addressing systematic delays between events in two series, will be kept zero throughout the remainder of this paper, since we will not be specifically interested in exploring time-delayed interactions between the variables of interest.

B. Partial event coincidence analysis

The analysis of bivariate event coincidence strengths Q_{ij} can be extended to n simultaneously observed event time series in a straightforward manner, which results in a symmetric bivariate event coincidence strength matrix,

$$\mathbf{Q} = \begin{pmatrix} 1 & Q_{1,2} & \cdots & Q_{1,n} \\ Q_{1,2} & 1 & \cdots & Q_{2,n} \\ \vdots & \vdots & \ddots & \vdots \\ Q_{1,n} & Q_{2,n} & \cdots & 1 \end{pmatrix}. \quad (3)$$

In full analogy with the established partial phase synchronization/coherence, we employ the matrix inversion of $\mathbf{Q}$ in order to define the partial event coincidence strength $Q_{i,j}^P$ between i and j as

$$Q_{i,j}^P = Q_{i,j|\{k\}} = |Q_{i,j}^{-1}| \bigg/ \sqrt{Q_{ii}^{-1} Q_{jj}^{-1}}. \quad (4)$$

This property can be interpreted as the residual probability of pairwise coincidences between events in two variables i and j when accounting for the probabilities of pairwise coincidences between events in i (j) and any of the remaining processes $k \neq i, j$, which is

not equivalent to the concept of conditional probabilities of event occurrences in the different variables. Accordingly, an indirect statistical association between i and j is indicated if the partial index $Q_{i,j}^P = Q_{i,j|\{k\}}$ approaches zero while the bivariate value Q_{ij} remains considerably different from zero, following the same rationale as for partial phase coherence analysis.[22]

We emphasize that the concept of partial event coincidence analysis (PECA) defined as above differs from the recently proposed extension of joint and conditional event coincidence analysis,[33] which accounts for a *specified* (sub)set of conditioning variables in the computation of bivariate event coincidence rates and generally comes with additional choices regarding the relative timings of events in the contributing time series. The latter approach, which explicitly draws on conditional probabilities of event occurrences in more than two variables, appears unfeasible in the presence of a larger number of interacting units or variables.

C. Effects of spatial embedding

Indirect connections appear frequently in spatially embedded topologies that are common in, e.g., brain networks. In order to account for this effect, we suggest to define a wiring cost by additionally considering the effect of spatial distance. Specifically, the proposed wiring cost $W_{i,j}$ between two time series representing two brain regions is defined as the product between the spatial distance and functional association strength, i.e., combining a physical Euclidean distance $D_{i,j}$ and the functional connectivity as expressed by $Q_{i,j}$, as

$$W_{i,j} = D_{i,j} \cdot Q_{i,j}. \quad (5)$$

For the case of the generic coupling structures shown in Fig. 1, we consider a two-dimensional embedding of the graphs. Assuming links with unit length, we then have three distinct distance values $(1, \sqrt{2}, 2)$ for the star and four $(1, 2, 3, 4)$ for the chain. It is straightforward to see that two brain regions with high event coincidence strength and large mutual separation yield a particularly large wiring cost.

As we will demonstrate below, using the classical bivariate measure $Q_{i,j}$ can result in false positive connections between two regions due to the presence of indirect interactions. To account for this, we further compute the partial wiring cost

$$W_{i,j}^P = D_{i,j} \cdot Q_{i,j}^P, \quad (6)$$

which takes small values for indirect connections because $Q_{i,j}^P$ is about zero.

D. Significance test

We justify the statistical significance of the results by surrogate data approaches. In particular, we test the null hypothesis that the event time series i is independent of j. For this purpose, we draw upon the concept of surrogate data. One corresponding possibility is to directly construct surrogate event series by randomizing the timings of events while keeping the waiting time distribution between subsequent events unchanged. For the numerical examples discussed in Sec. III, these resampling based surrogate event

sequences may, however, not appropriately represent the intrinsic dynamics of the coupled subsystems, which is why we take a different approach of generating independent realizations of twin surrogates with different initial conditions[34] and subsequently apply the same event definition as for the original data to the accordingly generated surrogate time series.

For each series under study, we accordingly generate 1000 surrogates event time series denoted by j^s ($s = 1, \ldots, 1000$) and compute the event coincidence strength Q_{ij}^s between each pair of i and j^s. The original Q_{ij} is considered significant at a 99% confidence level if it exceeds the empirical 99th percentile of the values obtained from the surrogate ensemble.

III. NUMERICAL EXAMPLES

A. Coupling identification based on partial event coincidence and partial phase synchronization

As a minimal example, we first study a simple three-node network (Fig. 2) of coupled nonlinear oscillators, which has been used as an example in similar previous studies.[21,22] Following the same numerical settings as in Schelter et al.,[21] we consider chaotic Rössler systems with additional independent white noises in their x components, which are diffusively coupled via their respective x components, described by the following governing equations:

$$
\xi_i : \begin{cases} \dot{x}_i = -\omega_i y_i - z_i + \sum_{j \neq i} \kappa_{i,j}(x_j - x_i) + \sigma_i \eta_i, \\ \dot{y}_i = \omega_i x_i + 0.15 y_i, \\ \dot{z}_i = 0.2 + z_i(x_i - 10.0), \end{cases} \tag{7}
$$

where $i, j = 1, 2, 3$, $\omega_1 = 1.03$, and $\omega_{2,3} = 1.01$ are the natural frequencies of the individual systems, and η_i are independent Gaussian distributed noise terms with zero mean and a standard deviation of $\sigma_i = 1.5$. The reason for choosing noisy chaotic oscillators is that without additional noise, the coupled Rössler oscillators would experience phase synchronization already at relatively small coupling strengths, while the additional noise terms elevate this synchronization threshold and, therefore, result in a larger interval of coupling strengths in which we can expect to be able to properly distinguish direct from indirect coupling. In addition, we note that since the considered noise only acts on the x components of the coupled oscillators, we do not use the standard notation of stochastic differential
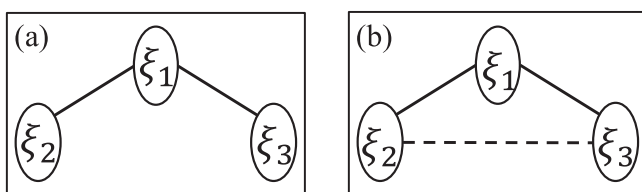
equations, but stick to the above formulation as also used in previous works.[21]

We consider a bidirectional symmetric coupling with coupling strength $\kappa_{1,3} = \kappa_{3,1}$ between oscillators ξ_1 and ξ_3 and $\kappa_{1,2} = \kappa_{2,1}$ between ξ_1 and ξ_2. By contrast, the oscillators ξ_2 and ξ_3 are only indirectly coupled as realized by setting $\kappa_{2,3} = \kappa_{3,2} = 0$. We numerically integrate the system using a fourth-order Runge–Kutta method with random initial conditions and an integration step of $h = 0.01$. The first 10 000 data points are discarded as possible transients, and time series consisting of the subsequent $N = 100\,000$ data points are taken for our analysis.

To compare the results of our partial event coincidence analysis with an established benchmark, we consider partial phase synchronization analysis.[21] In this case, the bivariate event coincidence strength Q_{ij} is replaced by a phase coherence index R_{ij}, which is based on continuous phase variables for the different Rössler systems that can be defined in different ways.

1. Benchmark 1—Phase coherence based on x and y variables

Given that we have access to all three components of each Rössler system, R_{ij} is traditionally estimated in the following way.[25,35] We first define phase variables from the nonlinear oscillations of the individual systems based on their x and y variables, i.e., $\phi_i(t) = \arg(x_i(t) + \mathbf{i} y_i(t))$ with $\mathbf{i}$ denoting the imaginary unit and $\arg(\bullet)$ the phase angle of the complex argument, which is feasible since the individual Rössler systems are in their phase coherent regimes at the considered parameter values. These phase variables are then unwrapped to obtain continuous phase time series by taking the associated 2π periodicity into account. Based on these phase time series, the phase coherence index R_{ij} is estimated as $R_{ij} = |\frac{1}{T} \sum_{t=1}^{T} \exp(\mathbf{i}(\phi_i(t) - \phi_j(t)))|$, where T is the integration time (i.e., the number of time steps).

2. Benchmark 2—Phase coherence based on z variables

While the x and y variables of the considered Rössler oscillators exhibit well defined oscillations around a unique center (i.e., phase coherent dynamics), the z components display large spike-like excursions separating longer periods with $z(t) \approx 0$. This spiky and not quite oscillatory behavior renders it difficult to infer relevant information on the nonlinear dynamics of the Rössler system from its z component only, which lacks proper observability[36] limiting the identification of synchronization phenomena from the perspective of a time-continuous phase dynamics.[37] Despite these conceptual limitations, we can still perform phase synchronization analysis based on this variable when introducing a proper Poincaré section, i.e., identifying two consecutive crossings of a given threshold value as one cycle corresponding to a phase increment of 2π, and defining a continuous phase variable by linear interpolation in time, i.e., $\phi(t) = 2\pi k + 2\pi \frac{t - t_k}{t_{k+1} - t_k}$ for $t_k \leq t < t_{k+1}$, where t_k and t_{k+1} are the timings of two consecutive threshold crossings. This method is based on a uniform phase interpolation for each cycle between two consecutive crossings, which is feasible if the crossings appear relatively regularly in time like for the z component of the Rössler

FIG. 2. Illustrative example for direct and indirect interactions in a simplistic three-node network.[21] (a) Correct topology and (b) additional false positive connection as denoted by the dashed line which would be revealed by most bivariate statistical association measures.

system. However, it remains problematic to assign 2π increments for two consecutive spikes if the crossings are more heterogeneously distributed in time, e.g., in case of long quiescent intervals followed by a few non-uniform spikes.

Event based similarity concepts like event synchronization[38] and event coincidence analysis provide solutions to tackle the challenge of studying synchrony between Rössler systems based on their z variables only by characterizing the statistical interdependence between two spike trains, making the explicit definition of a continuous phase variable unnecessary. Here, we obtain event time series defined by threshold crossings when the z component becomes larger than $z_e = \bar{z} + 1.8\sigma_z$, where $\bar{z}$ and σ_z are the empirical mean value and standard deviation of the z variable, respectively.

For the three noisy Rössler systems coupled as shown in Fig. 2(a), we independently vary the symmetric coupling strengths between ξ_1 and ξ_2 as well as between ξ_1 and ξ_3 in a range between 0 and 0.3, in which transitions to phase synchronization can be observed. For each pair of coupling strengths $\kappa_{1,2}$ and $\kappa_{1,3}$, we compute both the bivariate [Figs. 3(a)–3(c)] and the partial event coincidence strengths [Figs. 3(d)–3(f)]. The results agree remarkably well with those reported by Schelter et al.[21] for (partial) phase coherence. In particular, the bivariate analysis indicates significant coupling between ξ_1 and ξ_2 as well as between ξ_1 and ξ_3, but also shows substantial non-zero values of the event coincidence strength $Q_{2,3}$ between ξ_2 and ξ_3 [Fig. 3(c)], which corresponds to a false positive connection since ξ_2 and ξ_3 are only indirectly connected
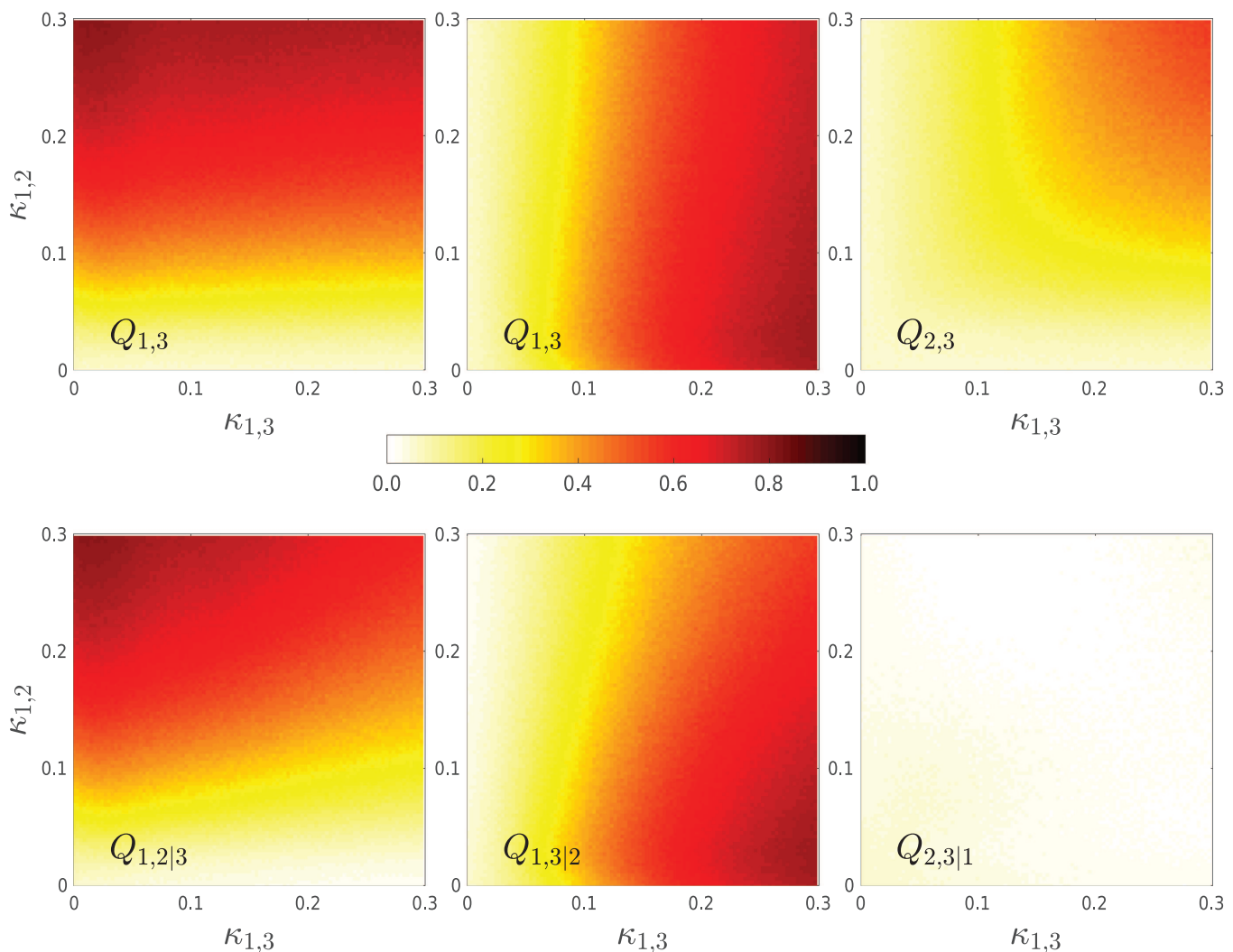

FIG. 3. Values of pairwise event coincidence strengths $Q_{i,j}$ and partial event coincidence strengths $Q_{i,j}^p$ in dependence on the two coupling strengths for the three noisy chaotic Rössler oscillators in the symmetric bidirectional coupling configuration shown in Fig. 2.

[Fig. 2(a)]. The bivariate analysis, hence, yields a spurious pseudo-connection between ξ_2 and ξ_3 [as highlighted in Fig. 2(b)], which originates from the common influence exerted by ξ_1 on the two other oscillators. By contrast, the partial event coincidence strengths $Q_{1,2}^P = Q_{1,2|3}$ and $Q_{1,3}^P = Q_{1,3|2}$ display essentially the same behavior as their direct bivariate counterparts, while $Q_{2,3}^P = Q_{2,3|1}$ takes far smaller values in the area of spurious synchronization. Therefore, this behavior strongly suggests that there is only an indirect coupling between ξ_2 and ξ_3, thereby excluding the false positive connection indicated by the dashed line in Fig. 2(b).

We further contrast the performance of PECA to distinguish the indirect coupling between ξ_2 and ξ_3 from the two direct connections with the respective results for the two partial phase synchronization based benchmark methods in the same range of coupling strengths. In Fig. 4, we show the empirical distributions of the three partial association measures evaluated over the whole range of considered coupling strengths [corresponding to Figs. 3(d)–3(f) and their respective counterparts]. For the direct connections, all three partial measures exhibit a significant frequency of non-zero values mainly associated with larger coupling strengths [Figs. 4(a) and 4(b)]. The observed differences among the three measures result from the spiking behavior of the z component of the chaotic Rössler systems. Notably, for the indirect coupling between ξ_2 and ξ_3, we find that the distribution of partial event coincidence strengths is concentrated more closely to zero than the values of the two partial phase coherence indicators [Fig. 4(c)]. However, performing a systematic quantitative inter-comparison between the respective performances of the different measures as discriminators between direct and indirect links would require a much more elaborate analysis strategy and is beyond the scope of the present work. To this end, we conclude that our approach based on the timing of specific events alone yields results that are greatly consistent with those of the classical methods requiring a continuous phase variable.

Finally, we show the dependence of the obtained results on the time series length N for an illustrative example of coupling strengths $\kappa_{1,2} = \kappa_{1,3} = 0.2$. As shown in Figs. 5(a) and 5(b), we find that both the direct bivariate and partial event coincidence strengths are significantly different from zero for the directly coupled oscillators. By contrast, the partial event coincidence strengths are close to zero for the indirectly interacting oscillators [Fig. 5(c)]. All those results converge as the time series length N is increased. Based on Fig. 5(c), we notice that the indirect coupling has been correctly identified for $N \gtrsim 1000$ (i.e., ≈ 5–6 oscillations of the Rössler systems). The same conclusion can be obtained for the (partial) phase coherence benchmark case 1 [Figs. 5(d)–5(f)]. However, for the corresponding benchmark case 2, we find that even longer series are required to obtain a clear distinction between direct and indirect coupling [Figs. 5(g)–5(i)].

B. Five coupled noisy Rössler systems

Next, we study the same type of coupled noisy Rössler oscillators as before (with independent Gaussian distributed white noise terms η_i with zero mean and a standard deviation of $\sigma_i = 1.5$), but considering five of such systems coupled as shown in Fig. 1. For the star configuration [Fig. 1(a)], we take the natural frequencies of the individual systems as $\omega_1 = 1.03$ and $\omega_2, \ldots, \omega_5 = 1.01$ and a bidirectional coupling of the same strength $\kappa_{1,j} = \kappa_{j,1} = \kappa$ between the hub ξ_1 and each leaf node $\xi_j, j = 2, \ldots, 5$. Note again that the oscillators on the leaf nodes $\xi_{2,\ldots,5}$ are indirectly coupled with each other, with a mutual flow of information mediated via the hub node ξ_1. When the five oscillators are coupled as a chain [Fig. 1(b)], we choose $\omega = 1.03$ for all nodes, while $\kappa = \kappa_{1,2} = \kappa_{2,1} = \kappa_{1,3} = \kappa_{3,1} = \kappa_{2,4} = \kappa_{4,2} = \kappa_{3,5} = \kappa_{5,3}$. Numerical integration and definition of events follow exactly the same procedure as described above. In
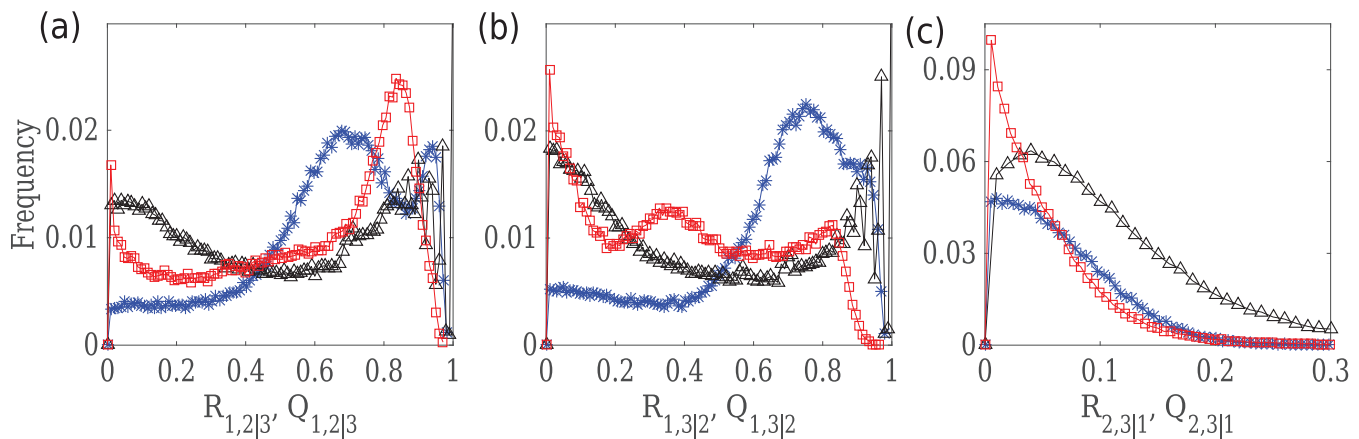

FIG. 4. Histograms of partial association strengths $R_{i,j|k}$ and $Q_{i,j|k}$ among the three coupled noisy Rössler oscillators for the direct connections between (a) ξ_1 and ξ_2 and (b) ξ_1 and ξ_3 and (c) the indirect connection between ξ_2 and ξ_3. Three different definitions of statistical associations are included: partial phase coherence index based on $\phi = \arctan y(t)/x(t)$ ($*$, blue) and phase increments of 2π between times at which the $z(t)$ variable shows crossings over a threshold ($\triangle$, black), and partial event coincidence strength ($\square$, red).
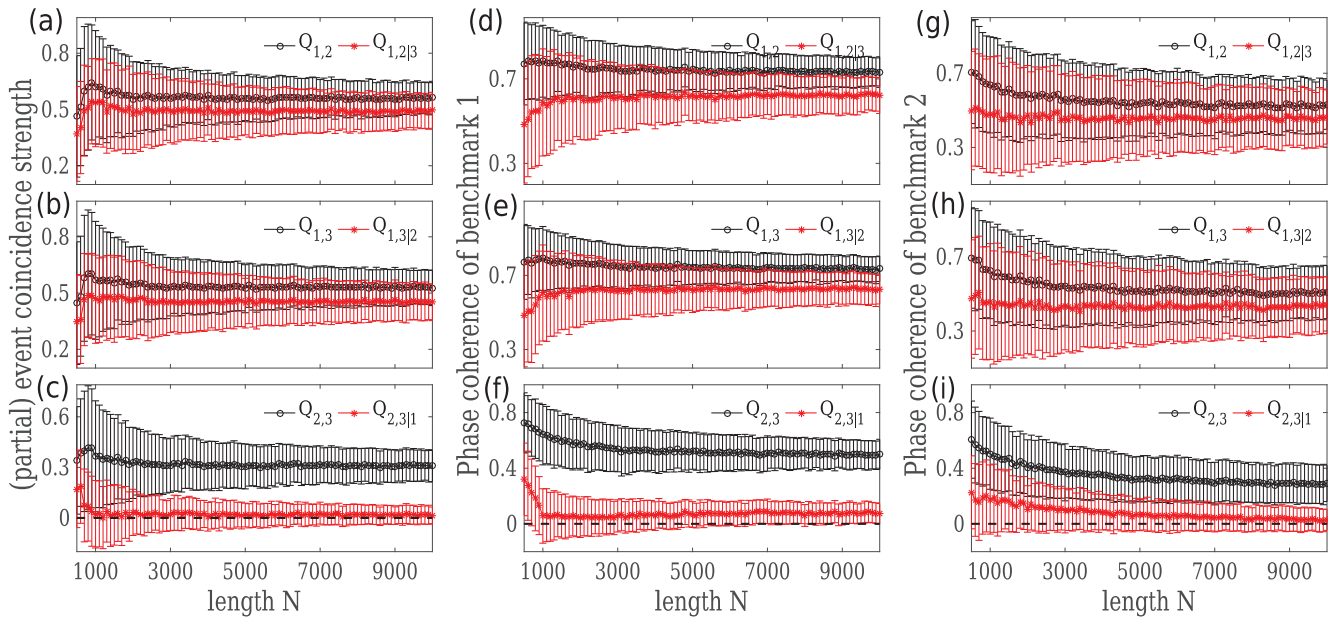
FIG. 5. Convergence of pairwise and partial association strengths $Q_{i,j}$ and $Q_{i,j|k}$ for the three coupled noisy Rössler systems. Values are based on event coincidence (a–c), and phase coherence of benchmark case 1 (d–f) , and benchmark case 2 (g–i). The shown error bars indicate the mean values and standard deviations obtained from 100 random realizations. Note that due to the strongly skewed distributions of the measures, some of the error bars reach out to negative values that are outside the admissible range of the considered measures.

the main text, we report the average results from 100 realizations with random initial conditions, while the corresponding standard deviations can be obtained from Figs. S1 and S2 in the supplementary material.

1. Star configuration

When applying direct bivariate event coincidence strengths Q_{ij} for functional network construction under the star configuration, the 99% significance level of the surrogate data test discussed in Sec. II D is exceeded for all pairs of nodes [Fig. 6(a)]. This means that in addition to the direct links between the hub and each of the leaves, additional indirect couplings among the leaf nodes are falsely identified as links. Specifically, the indirect connections between leaf nodes are identified if the coupling strength κ is larger than 0.1 [as shown in Fig. 6(a)]. Since all leaf nodes are identical except for their different initial conditions, the curves revealing the dependence on κ for bivariate analysis split into two groups: one group corresponds to the connections of any of the leaf nodes with the hub while the other group consists of pairs of leaf nodes.

When replacing the direct bivariate associations by partial event coincidence strengths ($Q_{i,j}^P = Q_{i,j|k}$), all false positive connections among the leaves are eliminated since they all fall below the corresponding significance level [Fig. 6(b)]. Note that, for small coupling $\kappa < 0.01$, neither bivariate nor partial ECA can reveal any connections between nodes simply because the interactions are not strong enough to be identified based on the available amount of events.

When the star network is additionally embedded in a two-dimensional Euclidean space, we use the wiring cost functions $W_{i,j}$ and $W_{i,j}^P$ to reflect the effect of this spatial embedding [Figs. 6(c) and 6(d)]. In this case, the bivariate analysis based on $W_{i,j}$ yields three groups corresponding to the three different Euclidean distances among nodes (Sec. II C), all of which exhibit partial event coincidence strengths above the considered significance threshold. By contrast, the partial wiring cost $W_{i,j}^P$ again successfully distinguishes indirect from direct couplings when $\kappa > 0.1$ (as highlighted by the background color in Fig. 6).

We note that while the above results correspond to the mean values of 100 realizations, there is a considerable spread between the individual values of (partial) event coincidence strengths among the realizations, leading to a few cases of overlapping error bars as shown in Fig. S1 in the supplementary material.

2. Chain configuration

For the chain configuration, the ten combinations of bivariate event coincidence strengths are divided into six groups because of the symmetry in the connections [Fig. 1(b); note that the oscillators are not numbered in consecutive order along the chain]. In particular, the six groups of bivariate curves are the following: $(Q_{1,2}, Q_{1,3})$, $(Q_{2,4}, Q_{3,5})$, $(Q_{1,4}, Q_{1,5})$, $(Q_{2,5}, Q_{3,4})$, $Q_{2,3}$, and $Q_{4,5}$. Among all pairwise connections, the weakest pseudo link between ξ_4 and ξ_5 is established when $\kappa > 0.2$ [Fig. 7(a)]. Again, all false positive connections are eliminated by considering partial event coincidence strengths whose values always remain clearly below the significance
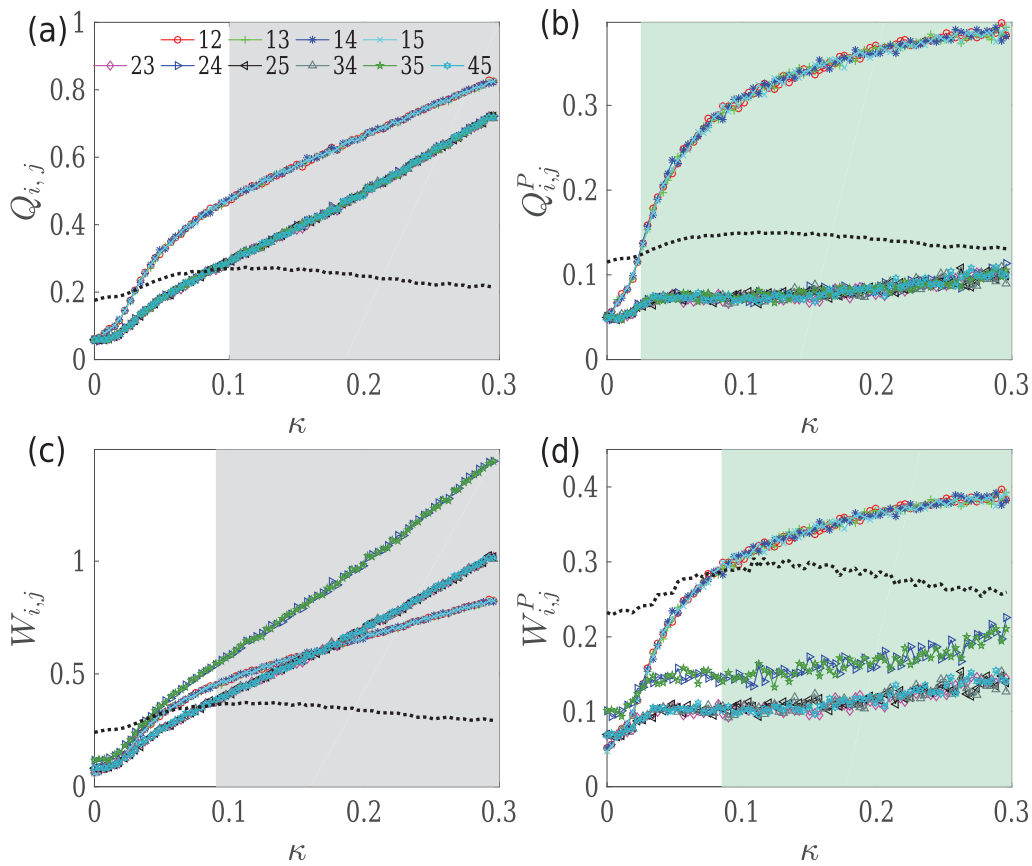
FIG. 6. Event based coupling inference for five coupled noisy Rössler oscillators on a star network without (a) and (b) and with two-dimensional spatial embedding (c) and (d) as the coupling strength κ is increased. (a) Bivariate event coincidence strength $Q_{i,j}$, (b) partial event coincidence strength $Q_{i,j}^P$, (c) direct wiring cost $W_{i,j}$, and (d) partial wiring cost $W_{i,j}^P$. Dotted lines indicate the 99% significance levels obtained from surrogate event time series with conserved waiting time distributions. The shaded gray backgrounds in panels (a) and (c) highlight cases with false positive connections being observed, which correspond to indirect connections between nodes. By contrast, the shaded green backgrounds in panels (b) and (d) indicate the range of coupling strengths for which the network topology is correctly identified.

level, while the direct connections of $\xi_1 - \xi_2$, $\xi_1 - \xi_3$, $\xi_2 - \xi_4$, and $\xi_3 - \xi_5$ differ significantly from zero [Fig. 7(b)]. In full analogy, the partial wiring cost $W_{i,j}^P$ correctly eliminates the indirect linkages falsely identified by the direct bivariate wiring cost $W_{i,j}$ when the two-dimensional spatial embedding is taken into account [Figs. 7(c) and 7(d)].

C. Coupled stochastic processes

As a second numerical example, we use a simple first-order vector auto-regressive (VAR(1)) process consisting of five coupled AR(1) components as[29]

$$\xi_i : x_{i,t} = \varphi_i x_{i,t-1} + \sum_{j \neq i} \kappa_{i,j} x_{j,t-1} + \varepsilon_{i,t}, \qquad (8)$$

where $\kappa_{i,j}$ are again coupling parameters modeling cross-correlations among the components and φ_i are the lag-one auto-regressive parameters modeling serial correlations for the respective variables

x_i. The error terms $\varepsilon_{i,t}$ are standard normally distributed with zero mean and unit variance. In the case of a star configuration [Fig. 1(a)], we choose $\varphi_1 = 0.2$, $\varphi_i = 0.4$ $(i = 2, 3, 4, 5)$ and $\kappa_{1,j} = \kappa_{j,1} = \kappa, j = 2, \ldots, 5$ and $\kappa_{i,j} = 0, i \neq 1$. For the chain model [Fig. 1(b)], we choose $\varphi_i = 0.45$ and the same symmetric coupling strength κ for each prescribed existing connection.

We emphasize that this second numerical example is drawn on purpose from a very different type of dynamical system as compared to the coupled noisy Rössler oscillators in order to demonstrate the general applicability of our event coincidence based framework to a great variety of different types of systems. It shall be noted that the correct coupling of the VAR model can be inferred from the explicit time series data by means of direct parameter estimation or other standard statistical inference techniques, while we are here interested in how well the same problem can be addressed based solely on the timing of specific events in each component, a problem addressed so far to our best knowledge only for a simple bivariate case.[29]
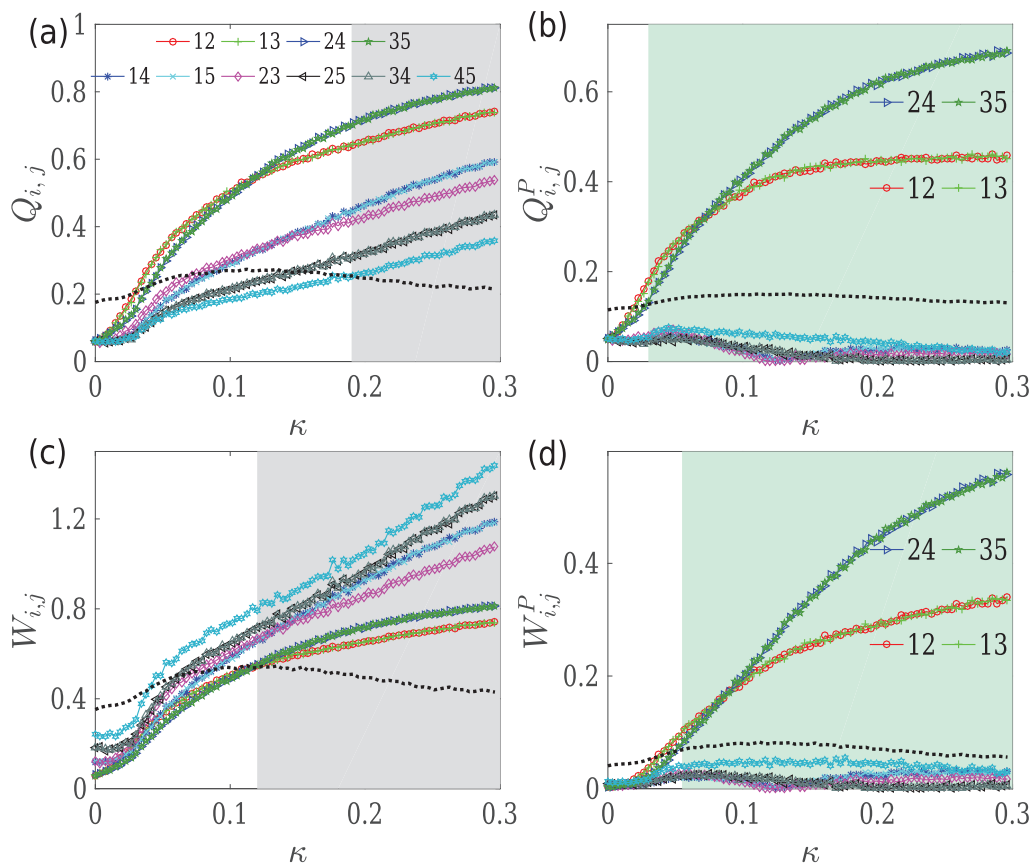
FIG. 7. Same caption as in Fig. 6, but for five coupled noisy chaotic Rössler oscillators on a chain.

By numerically simulating the model described above, we obtain five event time series when the simulated process values become larger than a given percentile of the underlying empirical distribution of the process. Specifically, we simulate the model to create 10 000 time points and use the empirical 90th percentile as a threshold, which yields about 1000 events for each series. Then, we calculate the bivariate coincidence strength $Q_{i,j}$ for $\xi_1, \ldots, \xi_5$[29] and the partial coincidence strength $Q_{i,j}^P$ while the coupling strength κ is systematically increased from 0 to 0.3.

We note that further numerical results (not shown) have demonstrated that we approach almost perfectly synchronized events (i.e., very high bivariate event coincidence strengths) among all coupled variables if the VAR(1) process is characterized by very strong coupling ($\kappa > 0.35$). In such a situation, the matrix of pairwise event coincidence strengths becomes gradually less well-conditioned so that the matrix inversion required for computing the partial event coincidence strengths becomes numerically challenging. It can be expected that other coupling inference approaches, like such based on linear correlations and/or regression models, will suffer from the same problem. As a result, similar as for chaotic oscillators experiencing (phase) synchronization, at high coupling strengths, we are not able to correctly identify the directly

coupled links anymore. Therefore, we restrict our analysis to coupling strengths $\kappa \in (0, 0.3)$ in Figs. 8 and 9. Again, we report the average results from 100 random realizations in the main text, while the corresponding standard deviations can be obtained from the error bars shown in Figs. S3 and S4 in the supplementary material.

1. Star configuration

Due to the stochastic nature of the processes, a narrow window of the coupling strength [$\kappa \in (0.23, 0.29)$] is identified based on bivariate event coincidence strength $Q_{i,j}$ within which we may observe qualitatively different significance results for different pairs of nodes [Fig. 8(a)]. By contrast, the partial event coincidence analysis $Q_{i,j}^P$ reveals a much larger interval of values of the coupling strength that allows excluding the effect of indirect connections among leaf nodes [$\kappa \in (0.18, 0.3)$ in Fig. 8(b)]. When additional spatial constraints are considered, the direct bivariate and partial wiring costs lead to rather similar results [Figs. 8(c) and 8(d)].

2. Chain configuration

For the chain topology, the direct bivariate analysis faces considerable challenges in establishing the connections unambiguously
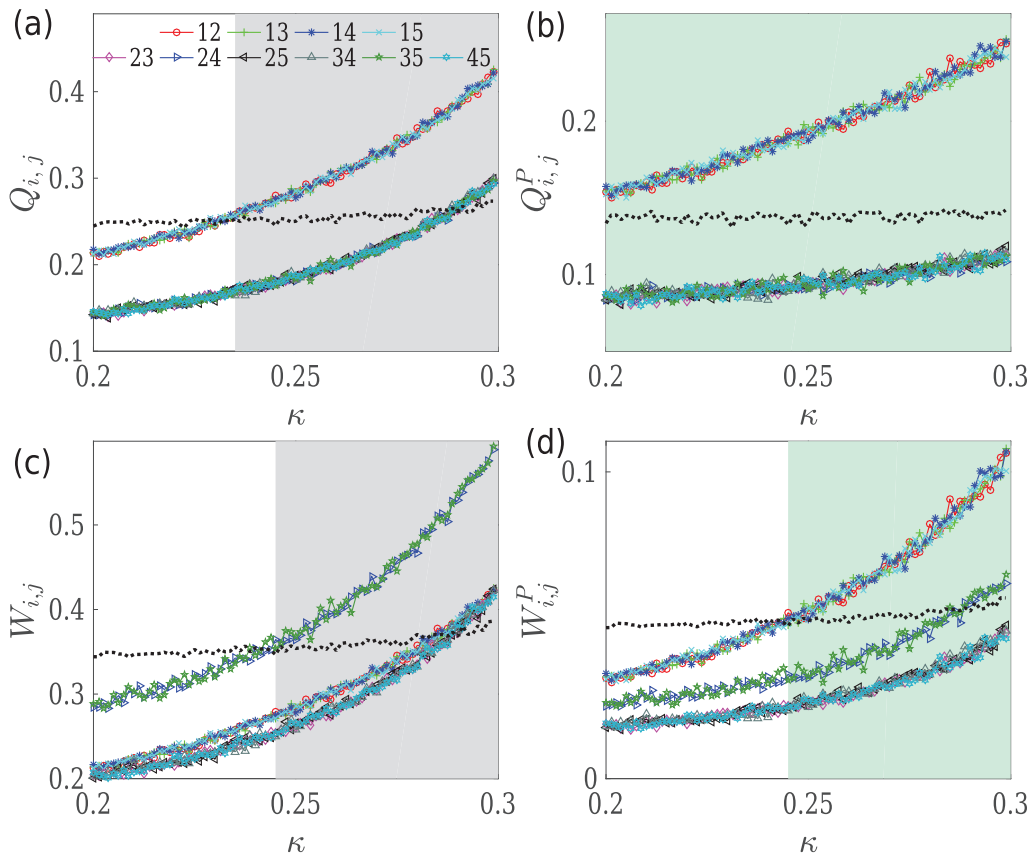
FIG. 8. Event based coupling inference for five coupled AR(1) processes on a star configuration without [(a) and (b)] and with two-dimensional spatial embedding [(c) and (d)]. (a) Bivariate event coincidence strength $Q_{i,j}$, (b) partial event coincidence strength $Q_{i,j}^P$, (c) direct wiring cost $W_{i,j}$, and (d) partial wiring cost $W_{i,j}^P$. Dotted lines correspond to the 99% significance level.

throughout the entire coupling interval, since most of the pairwise values remain below the significance level for a considerable range of coupling strengths. Moreover, the individual curves of $Q_{i,j}$ and $W_{i,j}$ exhibit a relatively wide spread without a clear gap between different groups of node pairs [Figs. 9(a) and 9(c)], which makes it hard to find a clear difference between direct and indirect couplings. By contrast, the partial measures $Q_{i,j}^P$ and $W_{i,j}^P$ indeed distinguish direct from indirect couplings; in particular, the directly interacting pairs $\xi_1 - \xi_2, \xi_1 - \xi_3, \xi_2 - \xi_4$, and $\xi_3 - \xi_5$ are well above the dashed lines indicating the significance level of the surrogate data based test while all other groups of indirect pairs clearly remain below these critical values [Figs. 9(b) and 9(d)].

IV. APPLICATION: ALPHA BAND FUNCTIONAL BRAIN CONNECTIVITY DURING DIFFERENT RESTING STATES

The numerical results discussed in Sec. III indicate that the partial event coincidence strength $Q_{i,j}^P$ and partial wiring cost $W_{i,j}^P$ are able to successfully distinguish direct from indirect connections. Specifically, we have demonstrated that the proposed method works in situations without and with explicit consideration of a spatial embedding of the nodes. As a real-world neurophysiological example, we finally report our corresponding results of an analysis of multi-channel human EEG recordings that unveils the functional connectivity patterns of the human brain during the two resting states with eyes closed (EC) and eyes open (EO) conditions. We specifically chose this application because it appears a non-typical case for the application of our methodology, since resting state EEG recordings are characterized by an absence of well distinguished activity spikes as commonly observed in task based EEG recordings or epileptic brain activity. We, therefore, consider the latter cases as examples our analysis methodology would be specifically tailored to, while it appears important to demonstrate that it can also provide useful results in a neurophysiological situation that would be typically investigated by other more established analysis approaches based on the full time series data.

A. Description of the data

We consider a set of publicly available 64-channel EEG recordings of 109 subjects (dataset 1) originally studied by Goldberger *et al.*[31] During the recordings, all subjects remained
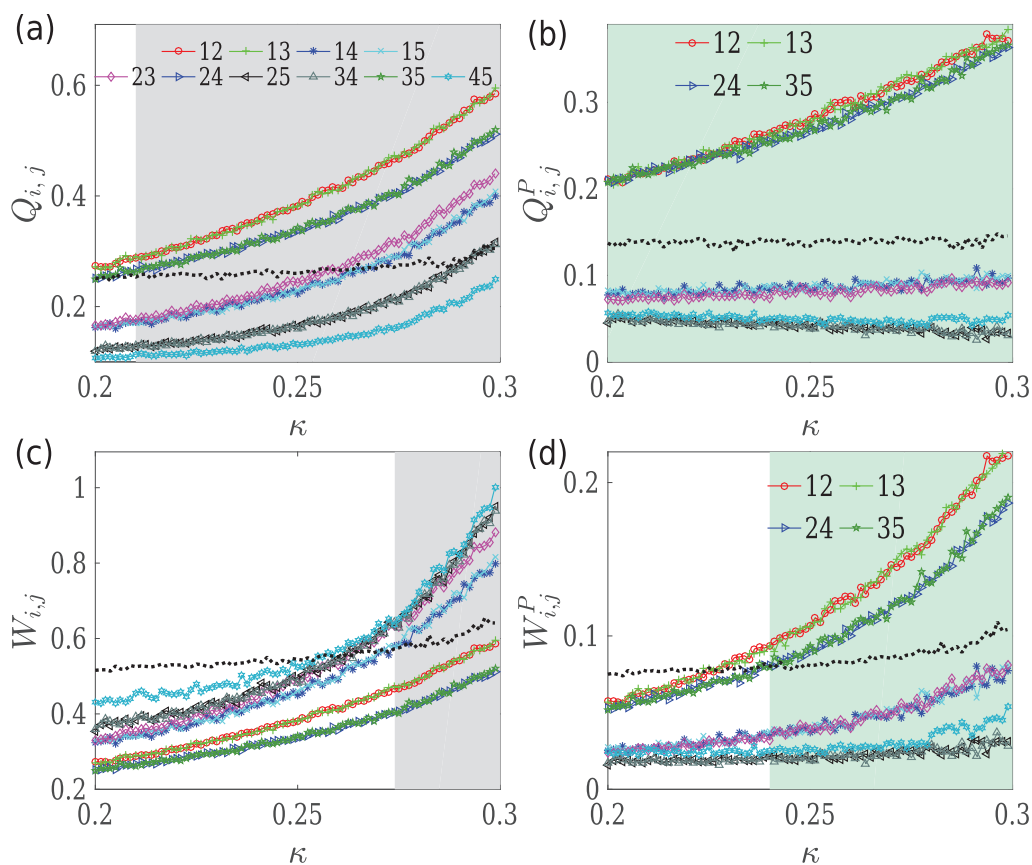
FIG. 9. Same as in Fig. 8, but for five coupled AR(1) processes on a chain without [(a) and (b)] and with two-dimensional spatial embedding [(c) and (d)]. Note that the curves obtained based on direct bivariate analysis exhibit a wide spread, which makes it hard to identify connections properly [(a) and (c)]. By contrast, $Q_{i,j}^P$ and $W_{i,j}^P$ reveal groups of nodes with partial statistical associations clearly above the significance level (indicating direct coupling) that are well separated from the others remaining below the significance level (indicating indirect coupling) [(b) and (d)].

at rest with one minute eyes closed and one minute eyes open condition. As necessary pre-processing steps, we removed artifacts related to eye blinks and eye movements following the standard procedure of Independent Component Analysis.[39,40] Complementary results for two other similar datasets (referred to as dataset 2 and dataset 3, respectively) are provided in the supplementary material.

It is well known that the alpha band is a predominant rhythm in the human brain, which has been investigated in studies of various cognitive processes.[32] Therefore, we apply bandpass filtering to the recordings at each individual EEG channel corresponding to the alpha band activity in the frequency band of (8, 13] Hz. Following the existing literature,[39,41] the considered EEG data are subsequently averaged over nine cerebral regions: left frontal (I), midline frontal (II), right frontal (III), left central (IV), midline central (V), right central (VI), left posterior (VII), midline posterior (VIII), and right posterior (IX), which are schematically shown in Fig. 10. Consistent results are obtained when the following steps are performed

on the 64 individual EEG channels as shown in the supplementary material.

Starting from the resulting nine time series $x_i(t)$ representing each of these brain regions, events are defined as the times when $x_i(t)$ crosses a threshold of $x_e = \bar{x} + 1.8\sigma_x$ from below, where $\bar{x}$ and σ_x are again the mean and standard deviation of the signal x. In case of consecutive time steps for which the signal exceeds this threshold, the first one is associated with the event. Next, we compute the matrix of event coincidence strengths **Q**. For defining wiring cost functions, normalized Euclidean distances (original distances divided by the overall maximum value) between the centers of the different brain areas are used, where for convenience a center has been defined as the mean of the three-dimensional positions of all electrodes associated with a given region on the scalp (and, hence, is generally located within the brain). Finally, we test the obtained values against the null hypothesis of statistical independence for each pair of event time series by using our surrogate data method on 99% significance level.
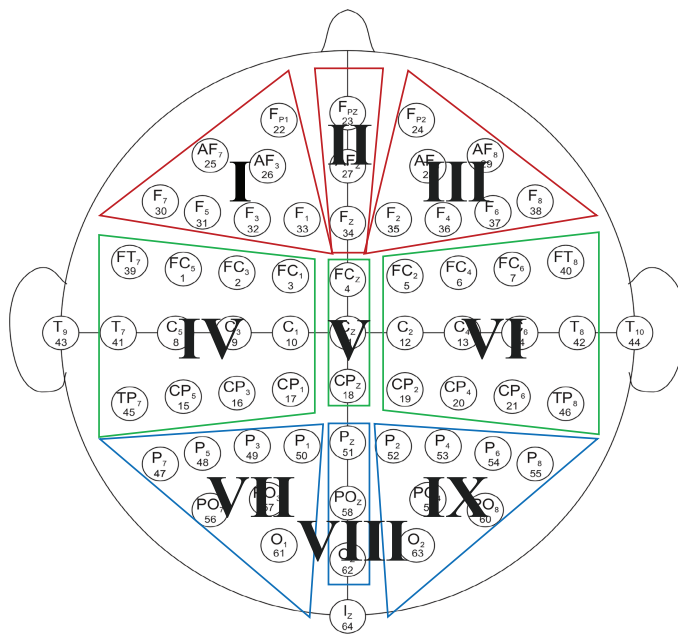
I: left frontal (LF)

II: middle frontal (MF)

III: right frontal (RF)

IV: left central (LC)

V: middle central (MC)

VI: right central (RC)

VII: left posterior (LP)

VIII: middle posterior (MP)

IX: right posterior (RP)

FIG. 10. Positions of electrodes and nine brain regions.

B. Functional connectivity estimation using ECA and PECA

When drawing upon the direct bivariate analysis, we find that different pairs of brain regions show different levels of generally strong (significant) mutual event synchrony. Specifically, all pairs among the nine brain regions exhibit statistically significant event coincidence strengths in the vast majority of cases for both types of conditions, indicating a fully coupled functional brain network [Figs. 11(a) and 12(a)]. Only in the EC state, we observe insignificant values of event coincidence strengths in more than 25% (but less than 50%) of all cases for just three pairs of regions: LF-RP, MF-RP, and RF-RP. Comparing both types of conditions [Fig. 11(a) vs Fig. 12(a)], we find that the magnitudes of pairwise event coincidence strengths in the EC state differ systematically from those during the EO state, which will be further analyzed below.

We next replace the classical bivariate measure by our new partial event coincidence strength. Indeed, accounting for the effect of any third brain regions on the statistical associations between functional activity in pairs of regions completely changes the overall picture as the majority of pairs now falls below the considered significance threshold. This indicates that many pairs of regions have been falsely identified by the direct bivariate approach but are actually only indirectly coupled. For EC conditions [Fig. 11(b)], this particularly applies to LF-MC, LF-RC, LF-LP, LF-MP, LF-RP, MF-LC, MF-RC, MF-LP, MF-MP, MF-RP, RF-LC, RF-LP, RF-MP, RF-RP, LC-MP, LC-RP, MC-LP, MC-RP, and RC-LP, while only the remaining pairs of regions appear as directly connected according to our partial event coincidence analysis (more than 50% but less than

70% of all subjects below the dashed line). Studying EO conditions leads to very similar results [Fig. 12(b)].

While Figs. 11 and 12 summarize the significance of pairwise statistical associations (as measured by both $Q_{i,j}$ and $Q_{i,j}^p$) among all subjects, it may be more convenient to further aggregate this information and project the mean behavior on the surface of the human brain. The corresponding spatial representation of the mean statistical associations further underlines that direct bivariate event coincidence strengths would indicate an almost fully connected network (including connections between both neighboring and distant brain regions), as shown in Figs. 13(a) and 13(b). By contrast, the partial event coincidence strengths identify direct connections to exist mainly between neighboring brain regions, but also (yet commonly weaker) between the left and right regions in the frontal, central, and posterior parts of the brain [Figs. 13(c) and 13(d)]. This implies that especially the apparent connections between frontal and posterior regions that are revealed by the direct bivariate associations are most likely of indirect nature and rather mediated via the central brain regions.

C. Connectivity strength under EO and EC conditions

Since the general functional brain connectivity patterns identified using our methodology do not differ qualitatively between EO and EC conditions, we next turn to the question whether or not there exist systematic quantitative differences between both states. As a first step of this analysis, we are primarily interested in the gross effect of experimental conditions on the synchrony of activity
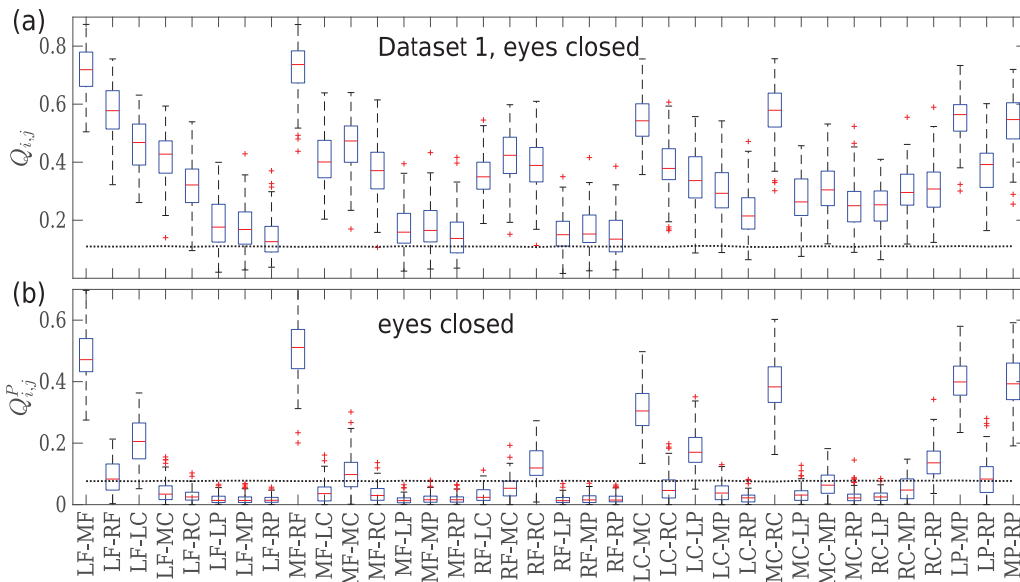
FIG. 11. Comparison between (a) direct bivariate ($Q_{i,j}$) and (b) partial event coincidence strengths ($Q_{i,j}^P$) for eyes closed condition. The dotted line indicates the 99% significance level of the surrogate data test. The bottom and top edges of each box indicate the 25th and 75th percentiles among the results for all studied patients, respectively, while the marker "+" symbolizes outliers.

between pairs of brain regions, irrespective of whether it originates from direct functional connections or collective effects mediated by other regions. In order to visualize the quantitative differences between the functional connection strengths under EC and EO conditions, we compute the event coincidence strength difference

$$DQ_{i,j} = Q_{i,j}^{EC} - Q_{i,j}^{EO}, \tag{9}$$

where the superscripts correspond to the EC and EO conditions, respectively, between all pairs of brain regions and plot them in the same way as before on a two-dimensional projection of the
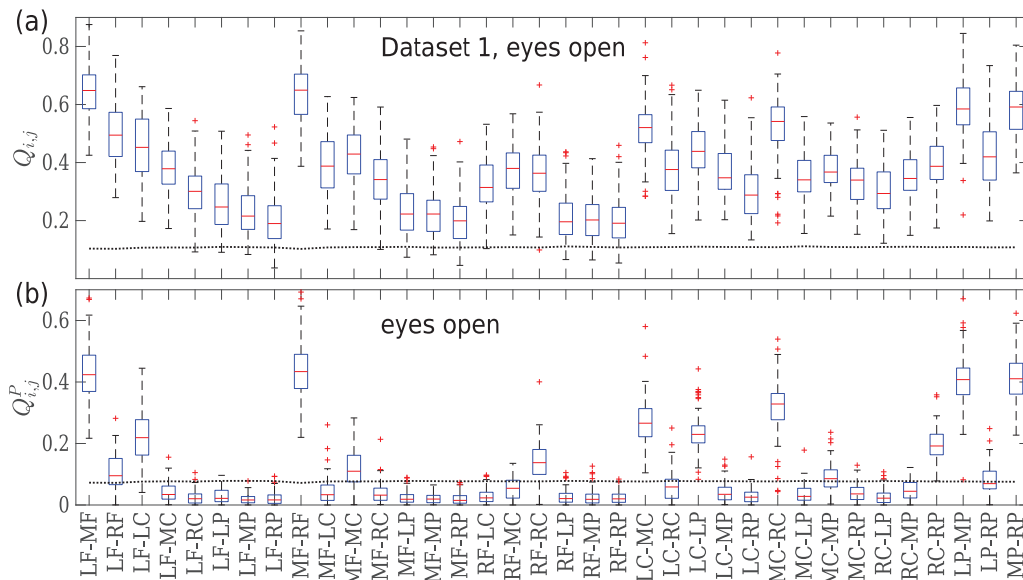

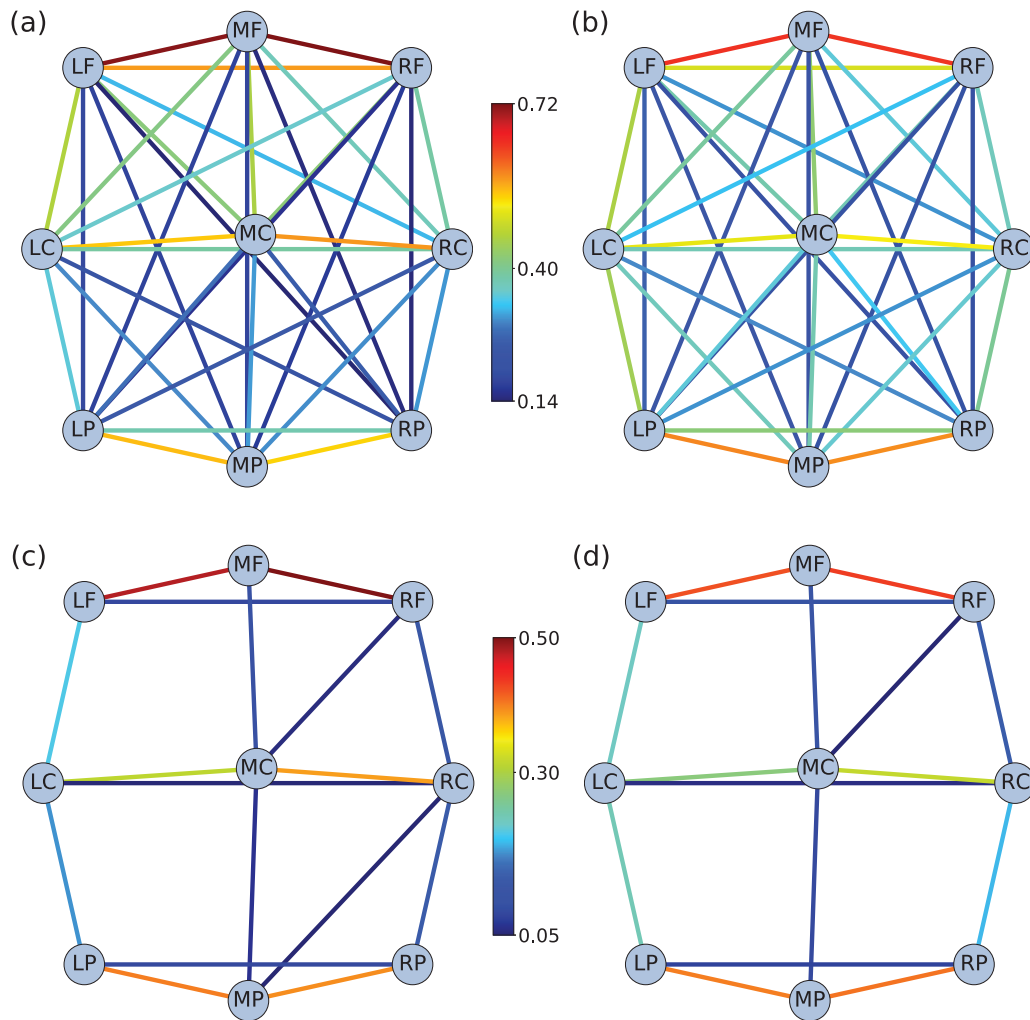**FIG. 12.** Same caption as in Fig. 11 but for eyes open condition.

FIG. 13. Summary of the spatial placement (two-dimensional brain projections as in Fig. 10) of significant statistical associations (colors indicating the mean values taken over all patients in the sample) among the nine macroscopic brain regions as identified by, respectively, [(a) and (b)] direct bivariate event coincidence strengths $Q_{i,j}$ and [(c) and (d)] partial event coincidence strengths $Q_{i,j}^{P}$ under [(a) and (c)] eyes closed and [(b) and (d)] eyes open condition.

human brain as shown in Fig. 14. Our definition implies that stronger total interdependencies under EC than under EO conditions are indicated by positive values of $DQ_{i,j}$, while negative $DQ_{i,j}$ values indicate stronger connections under EO than under EC conditions. As a result, we find a notable amount of consistently positive differences concentrated in the frontal brain regions (i.e., stronger connections during EC conditions) as shown in Fig. 14(a). By contrast, negative differences (i.e., stronger connections during EO conditions) are primarily found in the posterior regions [Fig. 14(b)].

For the sake of completeness, we also compute the corresponding partial event coincidence strength differences $DQ_{i,j}^{P}$ by replacing the direct bivariate associations in Eq. (9) by their partial

counterparts. The corresponding results are shown in Figs. 14(c) and 14(d). We find that under EC conditions, especially the connections of the middle frontal and central regions with their left and right counterparts are strengthened relative to EO conditions. The same also applies to the RC-MP connection, while the partial event coincidence strength differences for RP-LP and RF-MP are generally close to zero. By contrast, stronger connections under EO conditions are found (i) between the central regions and the frontal and posterior ones in the right, middle, and central parts of the brain, (ii) for the direct connections between left and right regions in the frontal and central parts of the brain, and (iii) between the middle posterior region and its left and right counterparts. In summary, we still find that stronger connections under EC conditions
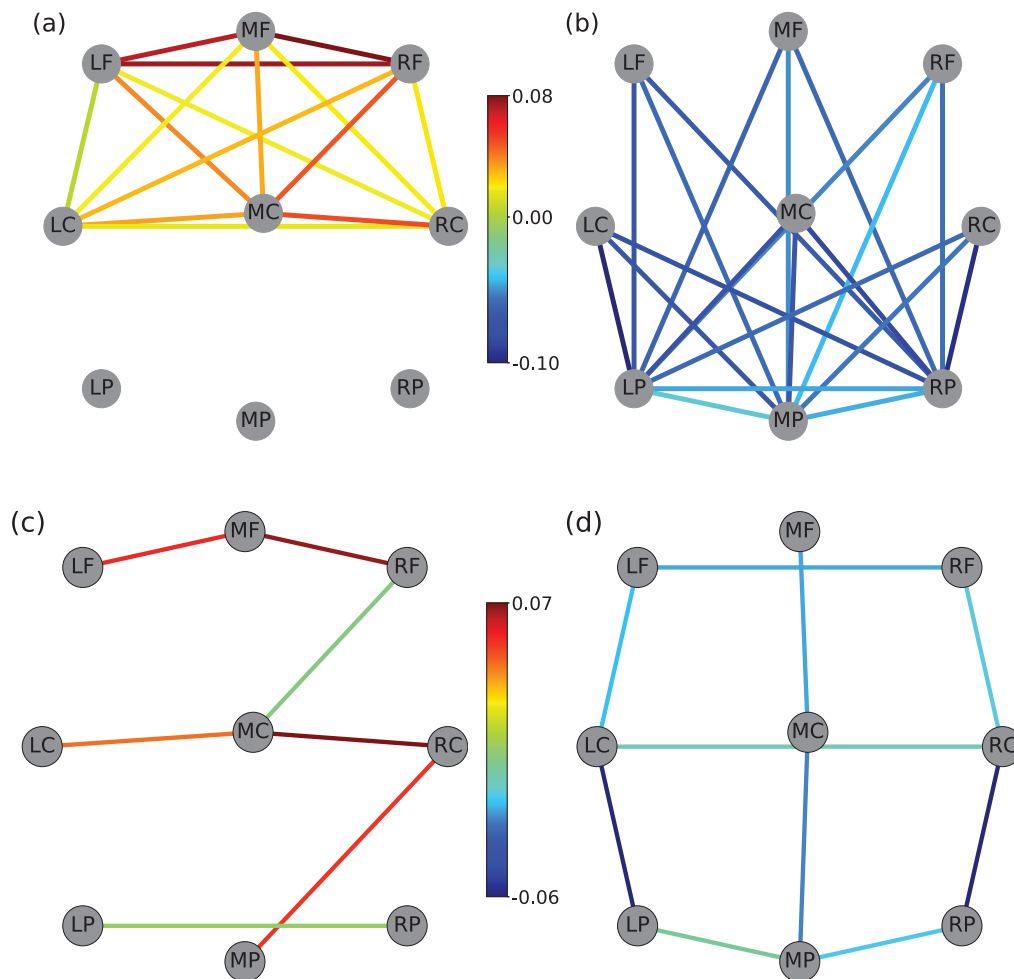
FIG. 14. Differences of [(a) and (b)] event coincidence strengths and [(c) and (d)] partial event coincidence strengths between EC and EO conditions: positive values of (a) $DQ_{i,j}$ and (c) $DQ^P_{i,j}$ indicating stronger associations under EC conditions; negative values of (b) $DQ_{i,j}$ and (d) $DQ^P_{i,j}$, indicating stronger associations during EO conditions.

are mainly concentrated in the frontal and central parts of the brain, while EO conditions are characterized by stronger connectivity in the posterior regions and between the frontal, central, and posterior parts.

D. Effect of spatial embedding

Finally, we discuss the effects of spatial embedding on the coupling identification by computing the wiring costs between all pairs of brain regions for the EC and EO conditions, respectively.[42] As before, the wiring cost $W_{i,j}$ is defined as the direct product between the spatial distance and functional association, i.e., $W_{i,j} = D_{i,j}Q_{i,j}$ (see Sec. II C). This is motivated by an analogy with technological transportation system, where the construction cost of a physical link increases proportional to the covered distance and the accommodated traffic volume. Similar approaches can also be found in

the previous literature.[42] With our corresponding definition, it is straightforward to see that two further separated brain regions with stronger event coincidence strength yield a larger wiring cost for the information transfer. The overall global wiring cost W of a subject is simply defined as the average over all pairs of brain regions. We associate a larger wiring cost W with a more synchronous activity of the brain, which is captured by larger values in the connectivity matrix **Q**.

As shown in Fig. 14, there exist notable, yet mainly quantitative connectivity differences between EC and EO conditions. Specifically, for EC conditions stronger connections (as compared to EO conditions) are clustered in the frontal brain regions, leading to larger wiring costs. By contrast, for the EO state, stronger connectivity than for EC conditions is mainly found in the posterior regions. Figure 15(a) summarizes the resulting wiring cost differences $W^{EC} - W^{EO}$ between EC and EO conditions, demonstrating
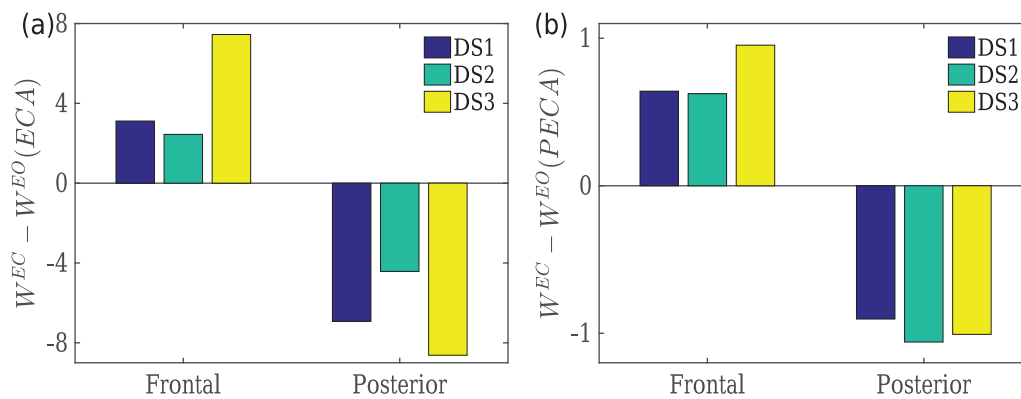
FIG. 15. Wiring cost differences between EC and EO conditions in the frontal and posterior brain regions, which are computed by (a) bivariate and (b) partial event coincidence strength.

that the frontal regions are highlighted by large positive cost differences while negative cost differences are mainly observed in the posterior regions. A qualitatively equivalent result is obtained for partial wiring cost differences based on partial event coincidence strengths [Fig. 15(b)].

V. CONCLUSIONS

We have generalized the concept of event coincidence analysis from a direct bivariate to a partial analysis method, which allows distinguishing direct from indirect coupling configurations based on the timing of events at mutually interacting dynamical units. Our method works both without and with explicit consideration of a possible spatial embedding of the network to be inferred, which has been demonstrated by simulating coupled noisy chaotic oscillators and stochastic processes on different paradigmatic network configurations. Specifically, our partial event coincidence analysis yields statistical association values that are narrowly distributed close to zero for the case of indirect connectivity, which suggests a very good discrimination between directly and indirectly connected units. Yet, the latter observation still has to be further supported by additional more systematic investigations with other established methods, which have been beyond the scope of the present work. To this end, we would like to express our confidence that, although we have focused in the present work on networks of small size, our method has great potential for identifying functional connectivity also in larger networks (see also some of the results shown in the supplementary material), since the computation of bivariate statistical associations and the subsequent matrix inversion operation can also be performed at reasonable computational costs for a larger number of interacting units.

From the application perspective, we have studied differences in the connectivity structures in the resting state human brain alpha band activity by the statistical measures of event coincidence strength and wiring cost computed for both eyes open (EO) and eyes closed (EC) conditions. In both brain states, we find that direct connections primarily exist between neighboring brain regions, while indirect links typically connect brain regions that are separated

by larger spatial distances. Compared to the connectivity pattern under EC conditions, we have demonstrated that EO conditions support stronger connections in the posterior brain areas, while EC conditions strengthen especially connections among the frontal areas. Both direct and indirect connectivity between the posterior and frontal areas are markedly enhanced in the presence of external visual stimuli processing during EO conditions. Therefore, our results comply with the alpha band desynchronization hypothesis in the posterior regions,[43] while providing a complementary perspective on the underlying processes that may be further exploited in future works to further improve our understanding of the underlying neurophysiological mechanisms.

In addition to the aforementioned neurophysiological perspectives of our proposed approach, there are also several methodological aspects that appear worth to be addressed in future work. While the need for a further thorough method inter-comparison has already been stressed, we particularly emphasize some possible modifications and extensions of our PECA. First, we have only considered instantaneous (lag-zero) coupling in our present study, which could be extended in a straightforward manner to an analysis of time-delayed coupling configurations. Second, we have defined event coincidence strengths based on pairs of trigger event coincidence rates. In the same spirit, we may also use precursor event coincidence rates or event coincidence rates based on symmetric coincidence windows. Understanding the advantages and disadvantages of either approach could help further optimizing the proposed methodology. Third, one may further consider exploiting the asymmetric nature of event coincidence rates for defining indicators of uni- vs bi-directional coupling. Ultimately, in the same spirit as for ECA, we may also generalize other related concepts like event synchronization, which has been widely used in neuroscience applications, to partial analysis methods. We are confident that these and further related methodological perspectives will also stimulate ample future work, for instance, a systematic comparative analysis with established methods like Granger causality, partial correlation analysis, and direct model inference (in the case of VAR model), but also model-free methods like time-delayed mutual information or transfer entropy.

SUPPLEMENTARY MATERIAL

See the supplementary material for additional error bar plots expanding Figs. 6–9 of the main text, which additionally indicate the standard deviations among the 100 considered random realizations. We further show that all the results reported in Sec. IV are qualitatively reproduced when considering two independent data sets of multi-channel EEG recordings. Moreover, the same sequence of analysis steps have also been performed based on the 64 individual EEG channels instead of their spatially aggregated versions, leading again to qualitatively consistent results as compared with those reported for the nine macroscopic brain regions.

ACKNOWLEDGMENTS

AUTHOR DECLARATIONS

Conflict of Interest

The authors have no conflicts to disclose.

DATA AVAILABILITY

The EEG data that support the findings of this study are publicly available in EEG Motor Movement/Imagery Database at https://www.physionet.org, Ref. 31.

REFERENCES

[1] S. Boccaletti, V. Latora, Y. Moreno, M. Chavez, and D.-U. Hwang, "Complex networks: Structure and dynamics," Phys. Rep. **424**, 175–308 (2006).
[2] M. E. J. Newman, "The structure and function of complex networks," SIAM Rev. **45**, 167–256 (2003).
[3] Y. Zou, R. V. Donner, N. Marwan, J. F. Donges, and J. Kurths, "Complex network approaches to nonlinear time series analysis," Phys. Rep. **787**, 1–97 (2019).
[4] E. Bullmore and O. Sporns, "Complex brain networks: Graph theoretical analysis of structural and functional systems," Nat. Rev. Neurosci. **10**, 186–98 (2009).
[5] K. Yamasaki, A. Gozolchiani, and S. Havlin, "Climate networks around the globe are significantly affected by El Niño," Phys. Rev. Lett. **100**, 228501 (2008).
[6] J. F. Donges, Y. Zou, N. Marwan, and J. Kurths, "The backbone of the climate network," Europhys. Lett. **87**, 48007 (2009).
[7] T. Rings and K. Lehnertz, "Distinguishing between direct and indirect directional couplings in large oscillator networks: Partial or non-partial phase analyses?," Chaos **26**, 093106 (2016).
[8] T. Stankovski, T. Pereira, P. V. E. McClintock, and A. Stefanovska, "Coupling functions: Universal insights into dynamical interaction mechanisms," Rev. Mod. Phys. **89**, 045001 (2017).
[9] N. Boers, B. Goswami, A. Rheinwalt, B. Bookhagen, B. Hoskins, and J. Kurths, "Complex networks reveal global pattern of extreme-rainfall teleconnections," Nature **566**, 373–377 (2019).
[10] J. Ludescher, M. Martin, N. Boers, A. Bunde, C. Ciemer, J. Fan, S. Havlin, M. Kretschmer, J. Kurths, J. Runge, V. Stolbova, E. Surovyatkina, and H. J. Schellnhuber, "Network-based forecasting of climate phenomena," Proc. Natl. Acad. Sci. U.S.A. **118**, e1922872118 (2021).
[11] V. M. Eguíluz, D. R. Chialvo, G. A. Cecchi, M. Baliki, and A. V. Apkarian, "Scale-free brain functional networks," Phys. Rev. Lett. **94**, 018102 (2005).

[12] R. Quian Quiroga, T. Kreuz, and P. Grassberger, "Event synchronization: A simple and fast method to measure synchronicity and time delay patterns," Phys. Rev. E **66**, 041904 (2002).
[13] M. Staniek and K. Lehnertz, "Symbolic transfer entropy," Phys. Rev. Lett. **100**, 158101 (2008).
[14] B. Barzel and A.-L. Barabási, "Network link prediction by global silencing of indirect correlations," Nat. Biotechnol. **31**, 720–725 (2013).
[15] N. Xiao, A. Zhou, M. L. Kempher, B. Y. Zhou, Z. J. Shi, M. Yuan, X. Guo, L. Wu, D. Ning, J. V. Nostrand, M. K. Firestone, and J. Zhou, "Disentangling direct from indirect relationships in association networks," Proc. Natl. Acad. Sci. U.S.A. **119**, e2109995119 (2022).
[16] J. Runge, V. Petoukhov, J. F. Donges, J. Hlinka, N. Jajcay, M. Vejmelka, D. Hartman, N. Marwan, M. Paluš, and J. Kurths, "Identifying causal gateways and mediators in complex spatio-temporal systems," Nat. Commun. **6**, 8502 (2015).
[17] J. Runge, "Causal network reconstruction from time series: From theoretical assumptions to practical estimation," Chaos **28**, 075310 (2018).
[18] S. T. Li, Y. Y. Xiao, D. Zhou, and D. Cai, "Causal inference in nonlinear systems: Granger causality versus time-delayed mutual information," Phys. Rev. E **97**, 052216 (2018).
[19] Y. Ruan, R. V. Donner, S. Guan, and Y. Zou, "Ordinal partition transition network based complexity measures for inferring coupling direction and delay from time series," Chaos **29**, 043111 (2019).
[20] N. P. Subramaniyam, R. V. Donner, D. Caron, G. Panuccio, and J. Hyttinen, "Causal coupling inference from multivariate time series based on ordinal partition transition networks," Nonlinear Dyn. **105**, 555–578 (2021).
[21] B. Schelter, M. Winterhalder, R. Dahlhaus, J. Kurths, and J. Timmer, "Partial phase synchronization for multivariate synchronizing systems," Phys. Rev. Lett. **96**, 208103 (2006).
[22] J. Nawrath, M. C. Romano, M. Thiel, I. Z. Kiss, M. Wickramasinghe, J. Timmer, J. Kurths, and B. Schelter, "Distinguishing direct from indirect interactions in oscillatory networks with multiple time scales," Phys. Rev. Lett. **104**, 038701 (2010).
[23] S. Porz, M. Kiel, and K. Lehnertz, "Can spurious indications for phase synchronization due to superimposed signals be avoided?," Chaos **24**, 033112 (2014).
[24] F. Hassanibesheli and R. V. Donner, "Network inference from the timing of events in coupled dynamical systems," Chaos **29**, 083125 (2019).
[25] A. Pikovsky, M. Rosenblum, and J. Kurths, *Synchronization—A Universal Concept in Nonlinear Sciences* (Cambridge University Press, 2001).
[26] J. F. Donges, C.-F. Schleussner, J. F. Siegmund, and R. V. Donner, "Event coincidence analysis for quantifying statistical interrelationships between event time series," Europ. Phys. J. S. T. **225**, 471–487 (2016).
[27] C.-F. Schleussner, J. F. Donges, R. V. Donner, and H. J. Schellnhuber, "Armed-conflict risks enhanced by climate-related disasters in ethnically fractionalized countries," Proc. Natl. Acad. Sci. U.S.A. **113**, 9216–9221 (2016).
[28] Z. Geng, Y. Zhang, B. Lu, J. Fan, Z. Zhao, and X. Chen, "Network-synchronization analysis reveals the weakening tropical circulations," Geophys. Res. Lett. **48**, e2021GL093582, https://doi.org/10.1029/2021GL093582 (2021).
[29] A. Odenweller and R. V. Donner, "Disentangling synchrony from serial dependency in paired-event time series," Phys. Rev. E **101**, 052213 (2020).
[30] F. Wolf, J. Bauer, N. Boers, and R. V. Donner, "Event synchrony measures for functional climate network analysis: A case study on South American rainfall dynamics," Chaos **30**, 033102 (2020).
[31] A. L. Goldberger, L. A. N. Amaral, L. Glass, J. M. Hausdorff, P. C. Ivanov, R. G. Mark, J. E. Mietus, G. B. Moody, C.-K. Peng, and H. E. Stanley, "PhysioBank, PhysioToolkit, and PhysioNet," Circulation **101**, e215–e220 (2000).
[32] M. Benedek, S. Bergner, T. Könen, A. Fink, and A. C. Neubauer, "EEG alpha synchronization is related to top-down processing in convergent and divergent thinking," Neuropsychologia **49**, 3505–3511 (2011).
[33] J. F. Siegmund, T. G. M. Sanders, I. Heinrich, E. van der Maaten, S. Simard, G. Helle, and R. V. Donner, "Meteorological drivers of extremes in daily stem radius variations of beech, oak, and pine in Northeastern Germany: An event coincidence analysis," Front. Plant Sci. **7**, 733 (2016).
[34] M. Thiel, M. C. Romano, J. Kurths, M. Rolfs, and R. Kliegl, "Twin surrogates to test for complex synchronisation," Europhys. Lett. **75**, 535–541 (2006).

[35]M. G. Rosenblum, A. S. Pikovsky, and J. Kurths, "Phase synchronization of chaotic oscillators," Phys. Rev. Lett. **76**, 1804–1807 (1996).

[36]L. A. Aguirre, L. L. Portes, and C. Letellier, "Structural, dynamical and symbolic observability: From dynamical systems to networks," PLoS One **13**, 1–21 (2018).

[37]L. A. Aguirre, L. L. Portes, and C. Letellier, "Observability and synchronization of neuron models," Chaos **27**, 103103 (2017).

[38]R. Quian Quiroga, T. Kreuz, and P. Grassberger, "Event synchronization: A simple and fast method to measure synchronicity and time delay patterns," Phys. Rev. E **66**, 41904 (2002).

[39]C. Quintero-Quiroz, L. Montesano, A. J. Pons, M. C. Torrent, J. García-Ojalvo, and C. Masoller, "Differentiating resting brain states using ordinal symbolic analysis," Chaos **28**, 106307 (2018).

[40]A. Mognon, J. Jovicich, L. Bruzzone, and M. Buiatti, "ADJUST: An automatic EEG artifact detector based on the joint use of spatial and temporal features," Psychophysiology **48**, 229–240 (2011).

[41]R. J. Barry, A. R. Clarke, S. J. Johnstone, C. A. Magee, and J. A. Rushby, "EEG differences between eyes-closed and eyes-open resting conditions," Clin. Neurophysiol. **118**, 2765–2773 (2007).

[42]J. Gómez-Ramírez, S. Freedman, D. Mateos, J. L. Pérez Velázquez, and T. A. Valiante, "Exploring the alpha desynchronization hypothesis in resting state networks with intracranial electroencephalography and wiring cost estimates," Sci. Rep. **7**, 15670 (2017).

[43]C. J. Stam, D. L. J. Tavy, and R. W. M. Keunen, "Quantification of alpha rhythm desynchronization using the acceleration spectrum entropy of the EEG," Clin. Electroencephalogr. **24**, 104–109 (1993).